ACS APPLIED MATERIALS & INTERFACES

Research Article

www.acsami.org

Shape-Controllable Gold Nanoparticle–MoS_2 Hybrids Prepared by Tuning Edge-Active Sites and Surface Structures of MoS_2 via Temporally Shaped Femtosecond Pulses

Pei Zuo,[†] Lan Jiang,*[,†] Xin Li,[†] Bo Li,[†] Yongda Xu,[†] Xuesong Shi,[†] Peng Ran,[†] Tianbao Ma,[§] Dawei Li,[∥] Liangti Qu,[‡] Yongfeng Lu,[∥] and Costas P. Grigoropoulos[⊥]

[†]Laser Micro/Nano Fabrication Laboratory, School of Mechanical Engineering, and [‡]Key Laboratory of Cluster Science, Ministry of Education, School of Chemistry, Beijing Institute of Technology, Beijing 100081, P. R. China

[§]State Key Laboratory of Tribology, Tsinghua University, Beijing 100084, P. R. China

[∥]Department of Electrical and Computer Engineering, University of Nebraska—Lincoln, Lincoln, Nebraska 68588-0511, United States

[⊥]Laser Thermal Lab, Department of Mechanical Engineering, University of California, Berkeley Berkeley, California 94720, United States

Supporting Information

ABSTRACT: Edge-active site control of MoS_2 is crucial for applications such as chemical catalysis, synthesis of functional composites, and biochemical sensing. This work presents a novel nonthermal method to simultaneously tune surface chemical (edge-active sites) and physical (surface periodic micro/nano structures) properties of MoS_2 using temporally shaped femtosecond pulses, through which shape-controlled gold nanoparticles are in situ and self-assembly grown on MoS_2 surfaces to form Au–MoS_2 hybrids. The edge-active sites with unbound sulfurs of laser-treated MoS_2 drive the reduction of gold nanoparticles, while the surface periodic structures of laser-treated MoS_2 assist the shape-controllable growth of gold nanoparticles. The proposed novel method highlights the broad application potential of MoS_2; for example, these Au–MoS_2 hybrids exhibit tunable and highly sensitive SERS activity with an enhancement factor up to 1.2×10^7, indicating the marked potential of MoS_2 in future chemical and biological sensing applications.

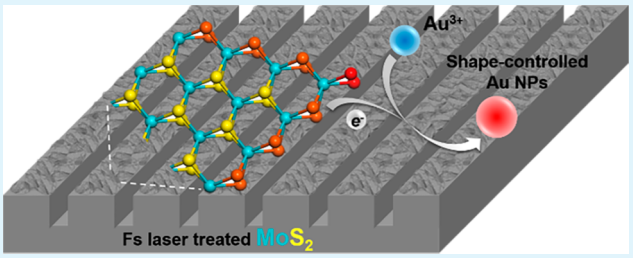

KEYWORDS: *MoS_2 film, shaped femtosecond pulse, edge-active site, periodic surface structure, Au–MoS_2 hybrids*

INTRODUCTION

Transition metal dichalcogenides, a group of graphene-like 2D crystals, display insulating, semiconducting, and metallic properties and can be applied to field-effect transistors, spin- and valleytronics, thermoelectrics, topological insulators, superconductors, etc.[1−4] A typical example from transition metal dichalcogenides family is molybdenum disulfide (MoS_2), which is a semiconducting crystal composed of a Mo layer sandwiched between two S layers, with the Mo in a trigonal biprism coordination.[5,6] The Mo and S atoms in the lamella are bonded by strong covalent force, while the interacting layers are connected through weakly van der Waals force.[5,6] Because of their low cost, earth abundance, high stability, and considerable chemical activity,[7] MoS_2 crystals have attracted substantial research interest and drawn increasing attention for applications in chemical catalysis,[8−10] synthesis of functional composites,[11,12] biochemical sensing,[13,14] and energy conversion.[15]

As is the case with many inorganic solids, pristine MoS_2 is relatively inert.[8] Its chemical catalytic activity is localized to rare surface sites, including defects on the basal plane and especially effective edge sites.[8−10,16] Hence, effective utilization and optimization of the chemical activity of MoS_2 is beholden to the challenges in tuning its edge-active sites. However, the research on tuning edge-active sites of MoS_2 remains inchoate and is only a recent effort. Recently, edge-active sites of MoS_2 have only be obtained during the preparation of MoS_2 sheets, through methods such as chemical deposition,[9,17,18] chemical synthesis,[8,19] or chemical exfoliation.[10,20] Although abundant edges can be obtained through chemical synthesis and exfoliation, both approaches suffer from disadvantages such as a demanding vacuum atmosphere, complex procedures, uncontrolled active degree, and contamination introduced by the processing chemicals; additionally, chemical deposition also faces low yield of edges and high operational cost. Therefore, it is necessary to develop a simple, green, economical, and tunable

Received: November 18, 2016
Accepted: February 3, 2017
Published: February 3, 2017

DOI: 10.1021/acsami.6b14805
ACS Appl. Mater. Interfaces 2017, 9, 7447−7455

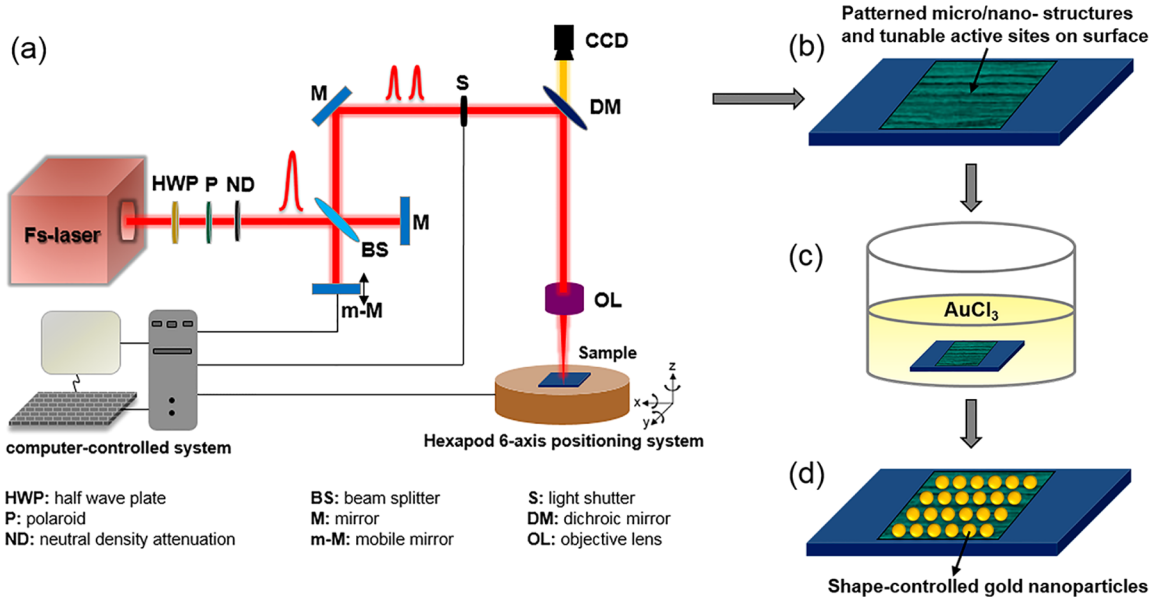

Figure 1. Schematic of experimental process. (a) Incident femtosecond pulse temporally shaped into double subpulses based on Michelson interferometer system. (b) Tunable active sites and micro/nano structures formed on MoS_2 film surface. (c) Modified MoS_2 film immersed in $AuCl_3$ solution. (d) Shape-controlled gold NPs decorated on treated MoS_2 film.

approach to obtaining edge sites while maintaining effective chemical activity.

Meanwhile, to improve the properties and expand the potential applications of MoS_2, MoS_2-based hybrid structures with foreign compositions have garnered extensive research interest. For example, MoS_2 composited with noble metal nanoparticles (NPs) can lead to local surface plasmon resonance (LSPR) for activating photo-electrocatalysis of hydrogen evolution and enhancing light emission or absorption of MoS_2, lead to surface-enhanced Raman scattering (SERS) for the application of chemical and biological sensing, and participate chemical reaction in electrochemical process for enhancing electrochemical performances of MoS_2.[21−30] For metal−MoS_2 hybrids, their performance and applications are largely affected by the intrinsic characteristic of the metal NPs, which are mainly determined by size, composition, crystallinity, and shape. In recent metal−MoS_2 hybrids, only metal NPs with single shape have been commonly obtained or utilized;[21−25] thus, the shape control of metal NPs on MoS_2 can be targeted for substantial improvement in the future. In addition, recent approaches to decorating metal NPs on MoS_2 are not in situ growth or require chemical reduction agents. For example, physical deposition, although which does not introduce additional species, requires a vacuum or inert atmosphere, and is not in situ growth, which might cause interface stress leading to lattice destabilization.[22,26,31] For the chemical methods, although they have advantages such as relatively low cost and high throughput, however, except necessary metal salts for providing metal cations, other chemical reagents are used.[21,23,24,32,33] These chemical reagents might bring reagent byproduct in reaction mixture, need to keep the purity and stability of reagents and take the solubility compatibility into account, and cause toxicity or chemical/environmental contamination.[34,35] Furthermore, the extra metal cations and organics might be absorbed on MoS_2 surface, resulting in MoS_2 property changes, such as the phase transition from semiconducting 2H-MoS_2 to metallic 1T-MoS_2 or the charge transfer between organic molecules and MoS_2 layer.[36,37] Finally, the traditional continuous laser method, which induces chemical activity of MoS_2 to obtain Au−MoS_2 hybrids, inevitably causes detrimental surface thermal oxidation of material at atmospheric environment because of the strong heating effect of a continuous laser.[25]

In this work, we proposed a novel method of utilizing temporally shaped femtosecond pulses to nonthermally tune edge-active sites (unbound sulfur) and surface periodic micro/nano structures on MoS_2 films. Various shape-controlled gold NPs were in situ self-assembly decorated on modified MoS_2 films in $AuCl_3$ solution without any reduction agents. Compared with previous reports, this method had advantages including simplicity, strong controllability, high efficiency, and absence of chemical contamination. Characterization analyses indicated that the chemical reduction ability of modified MoS_2 resulted from the sulfur-terminal edge-active sites. The shape control of the gold nanostructures was attributed to the effective simultaneous tuning of active sites and periodic micro/nano structures formed on MoS_2 films by temporally shaped femtosecond pulses. Compared with conventional femtosecond pulses, temporally shaped femtosecond pulses introduce higher ratio of unbound sulfur in MoS_2, leading to faster reaction rates and diversified shapes of gold NPs. The proposed method has excellent potential for use in chemical and biological sensing, activating photo-electrocatalysis of hydrogen evolution, and enhancing light emission or absorption of MoS_2; for example, the Au−MoS_2 hybrids exhibited highly sensitive and tunable SERS activity (Figure S1).

RESULTS AND DISCUSSION

In this work, smooth MoS_2 films were mechanically exfoliated from a natural crystal by using adhesive tape and tweezers, and Figures S2−S6 illustrate the characterizations about the size, thickness, and quality of these MoS_2 films. The schematic illustration of our method for decorating MoS_2 with shape-controlled gold NPs is shown in Figure 1, and the detailed illustration is provided in the Methods section. Briefly, a linearly polarized femtosecond laser beam (35 fs, 800 nm) was adopted

DOI: 10.1021/acsami.6b14805
ACS Appl. Mater. Interfaces 2017, 9, 7447−7455

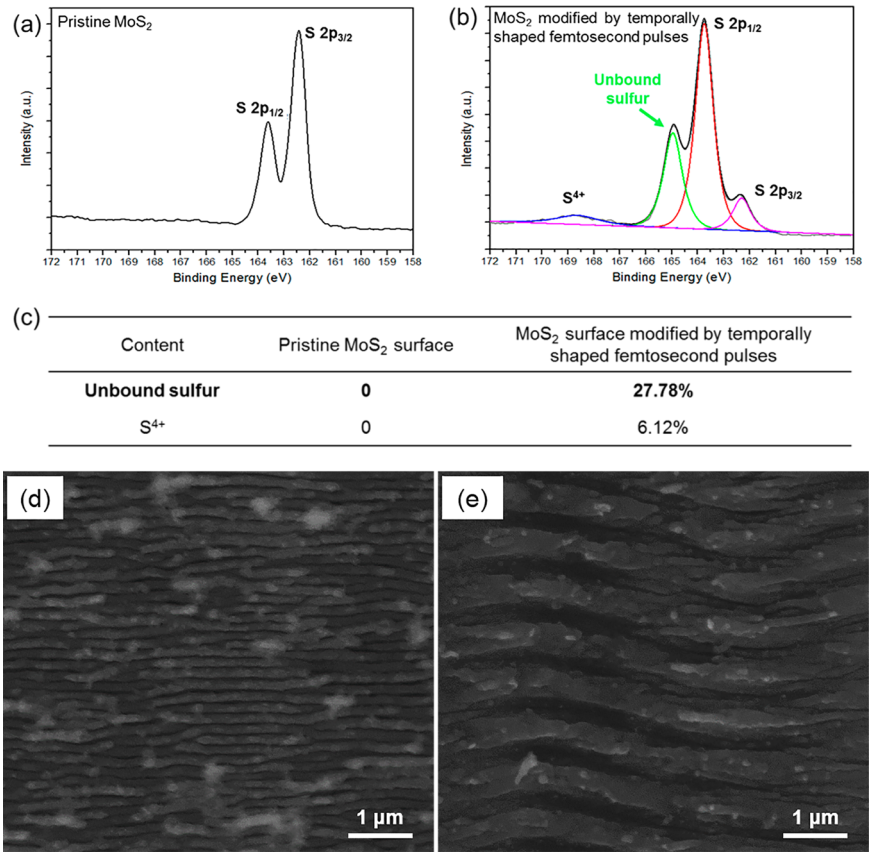

Content	Pristine MoS_2 surface	MoS_2 surface modified by temporally shaped femtosecond pulses
Unbound sulfur	**0**	**27.78%**
S^{4+}	0	6.12%

Figure 2. XPS S 2p spectral analyses and surface periodic micro/nano structures formed on laser-treated MoS_2. S 2p spectra for (a) pristine MoS_2 and (b) MoS_2 modified by temporally shaped femtosecond pulses. (c) Comparison of the contents of sulfur atoms (%) assigned to unbound sulfur and S^{4+} for pristine MoS_2 and MoS_2 modified by temporally shaped femtosecond pulses. (d) Short-periodic structures with period of 170 nm and (e) long-periodic structures with period of 700 nm.

and further temporally shaped into double subpulses with a delay ranging from femtoseconds to tens of picoseconds based on Michelson interferometer system for MoS_2 film surface processing (Figure 1a). Patterned micro/nano structures and tunable active sites were first simultaneously formed on laser-treated MoS_2 surfaces (Figure 1b). Next, the premodified MoS_2 films were directly immersed in $AuCl_3$ solution (Figure 1c), where gold cations were reduced within the modified regions and shape-controlled gold NPs were in situ and self-assembly decorated on MoS_2 film surfaces. After 30 min, MoS_2 films decorated with gold NPs were taken out for natural air drying (Figure 1d).

Surface Chemical and Physical Property Changes of Laser-Treated MoS_2. To investigate the physicochemical modification of MoS_2 films treated by femtosecond pulses, Raman spectroscopy, X-ray photoelectron spectroscopy (XPS), scanning electron microscope (SEM), and atomic force microscope (AFM) were employed. Figure S7 compares the Raman spectra of MoS_2 films with and without modification by femtosecond pulses. Two Raman-active modes were detected in MoS_2, $E_{2g}{}^1$ and A_{1g}, where the $E_{2g}{}^1$, in-plane mode results from the opposite vibration of two S atoms with respect to the Mo between them, and the A_{1g} mode results from the out-of-plane vibration of only S atoms in opposite directions.[38] A slight increase in the relative intensity of the A_{1g} mode was detected on the modified MoS_2 surface, which might be attributed to some kind of adsorbents on the modified MoS_2 surface, because the A_{1g} mode is very sensitive to the adsorbents on MoS_2 surface as well as electron doping.[38] Notably, there was no peak at 820 cm^{-1} originating from MoO_3 in Raman spectra, indicating no thermal oxidation for modified MoS_2[39] due to the advantage of nonthermal effect of femtosecond pulses.[40,41]

The detailed surface chemical modification of MoS_2 was further explored by XPS. XPS S 2p spectra for pristine MoS_2 and MoS_2 modified by temporally shaped femtosecond pulses are shown in Figure 2a–c. The S 2p spectra for pristine MoS_2 (Figure 2a) show two peaks at 162.4 and 163.6 eV, attributed to the S $2p_{3/2}$ and S $2p_{1/2}$ orbitals of saturated divalent sulfur, respectively. However, the S 2p spectra for MoS_2 modified by temporally shaped femtosecond pulses (Figure 2b) reveal an increase in the relative intensity of binding peak at 163.6 eV (S $2p_{1/2}$) and the appearance of two extra peaks at 164.96 eV (green line) and 168.6 eV (blue line), except two intrinsic binding energy at 162.4 eV (magenta line) and 163.6 eV (red line). The extra binding peak at 164.96 eV is assigned to unbound sulfur[42] and probably resulted from the sulfur head groups of Mo–S hexagonal rings in MoS_2 (Figure 3e). The unbound sulfurs have unpaired electrons, forming unsaturated bonds, namely dangling bonds. Therefore, the MoS_2 surface modified by femtosecond pulses revealed chemical reduction activity, which drove the reduction of gold NPs from $AuCl_3$ solution. The extra weak peak at 168.6 eV is assigned to oxidized S^{4+}, indicating that a small amount of sulfurs were oxidized to SO_2 molecules at atmospheric environment.[43] The oxidized SO_2 molecules were absorbed on the modified MoS_2

DOI: 10.1021/acsami.6b14805
ACS Appl. Mater. Interfaces 2017, 9, 7447–7455

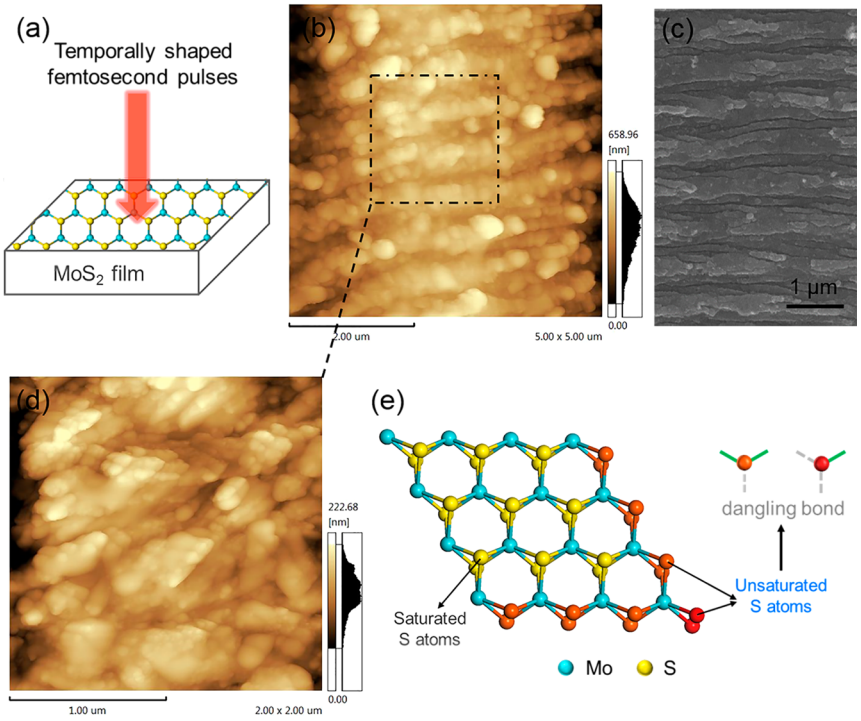

Figure 3. Mechanism of chemical reduction activity on MoS_2 surface induced by temporally shaped femtosecond pulses. (a) Schematic of femtosecond pulses irradiating on MoS_2 film. (b) AFM and (c) SEM images of periodic surface structures formed on modified MoS_2 film. (d) Enlarged AFM image of the marked micro area in (b), showing MoS_2 micro/nano debris. (e) Atomic scale schematic of the broken MoS_2 micro/nano debris.

surface, confirming our explanation for the detected increase of Raman A_{1g} intensity on modified MoS_2. By contrast, the S 2p spectra for MoS_2 modified by conventional femtosecond pulses (Figure S8a) show the same binding energy peaks as MoS_2 modified by temporally shaped femtosecond pulses. Figure 2c also provides the percent contents of sulfur atoms assigned to two extra binding energies by calculating the percent area of two peaks versus total spectrum. It should be noted that the content of unbound sulfur on MoS_2 surface modified by temporally shaped femtosecond pulses reached up to 27.78% (Figure 2c), which was observably higher than that by conventional femtosecond pulses of 21.74% (Figure S8b); this demonstrated higher chemical reduction activity of modified MoS_2 by temporally shaped femtosecond pulses. Additionally, a relatively lower content of oxidized S^{4+} on MoS_2 surface modified by temporally shaped femtosecond pulses (Figure 2c) than that by conventional femtosecond pulses (Figure S8b) further indicated higher chemical reduction activity of modified MoS_2 surface by temporally shaped femtosecond pulses because S^{4+} can impede the reduction of Au^{3+}. XPS Mo 3d spectra and analysis of pristine MoS_2 and MoS_2 modified by temporally shaped and conventional femtosecond pulses are shown in Figure S9.

Aside from surface chemical modification, two types of surface periodic micro/nano structures were formed on laser-treated MoS_2 (Figure 2d,e), respectively short-periodic structures with period of 170 nm and long-periodic structures with period of 700 nm. The chemical reduction activity of unbound sulfur formed on MoS_2 surface induced by temporally shaped femtosecond pulses is presented in Figure 3. Figure 3a shows the schematic of femtosecond pulses irradiating on MoS_2 film, and Figure 3d shows an enlarged AFM image of the marked MoS_2 micro area in Figure 3b, indicating the extreme roughness of the grating structure and the formation of abundant broken MoS_2 micro/nano debris. It was speculated that the MoS_2 micro/nano debris were defect-induced on each grating structure of the modified MoS_2 surface, and these MoS_2 micro/nano debris definitely terminates with S atoms,[44] as shown in Figure 3e. It can be seen that S atoms in MoS_2 molecule were marked by orange, dark orange, and red colors, corresponding to three-, two-, and one-coordination, respectively. The S atoms with coordination number less than three are unsaturated active S atoms with dangling bonds, which are considered to be the fundamental source for chemical activity and can reduce Au^{3+} ions. Specifically, the S atoms with one-coordination (red color) have the highest activity, followed by the S atoms with two-coordination (dark orange color); nevertheless, the S atoms with three-coordination (orange color) existing on pristine MoS_2 plane are saturated atoms with no chemical activity.[44]

Next, we explored how femtosecond laser increased the relative intensity of binding peak at 163.6 eV (S $2p_{1/2}$) and triggered the appearance of unbound sulfur peaking at 164.96 eV. When material is irradiated by ultrafast femtosecond laser with high power density and short pulse width, electrons are excited from bonding to antibonding states, and chemical bonds between atoms are instantaneously broken.[39,45,46] Hence, when femtosecond laser irradiating on MoS_2 surface, abundant Mo−S bonds (sharing electron pairs) were instantaneously weaken or even broken entirely. Then the valence state of abundant stimulated S atoms became higher, and the decrease of electrons provided by bonded Mo atoms led to a decrease of outer electrons density of S atoms and weaker shielding effect; thus, the binding energy of abundant S atoms integrally increased, and the relative intensity of binding peak at 163.6 eV (S $2p_{1/2}$) increased. When major chemical

DOI: 10.1021/acsami.6b14805
ACS Appl. Mater. Interfaces 2017, 9, 7447−7455

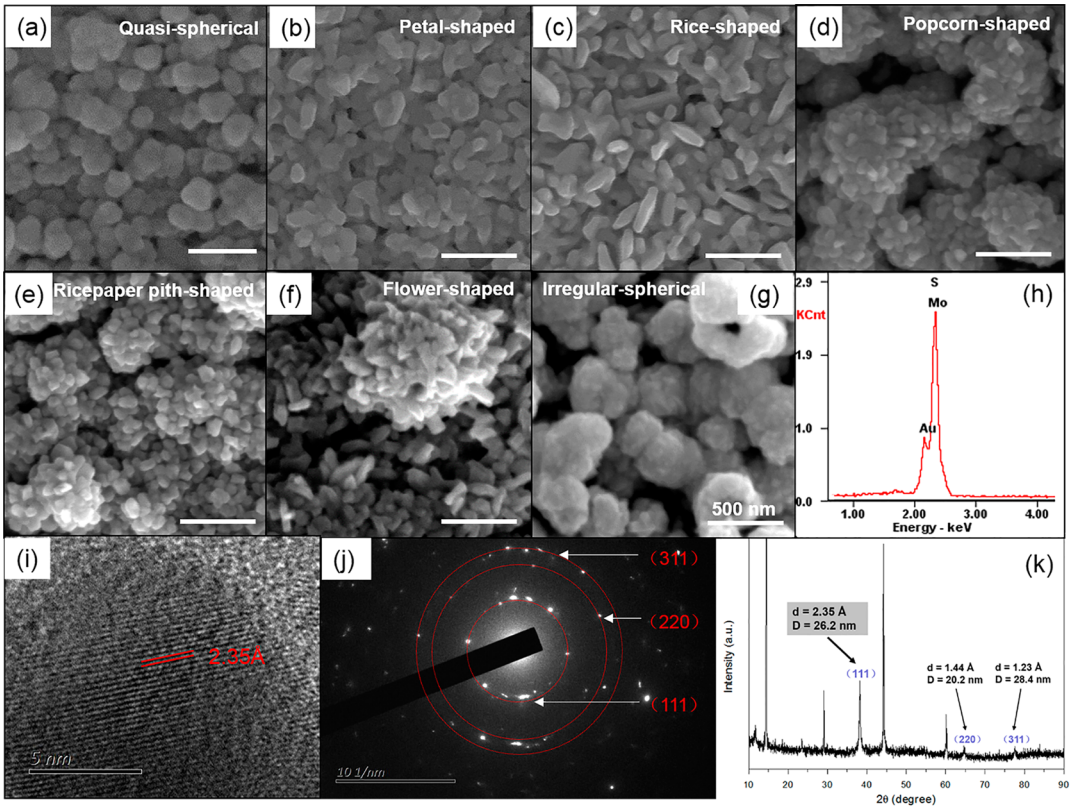

Figure 4. Systemic characterization of gold NPs decorated on MoS_2 films. (a–f) Typical SEM images of six kinds of gold NPs on MoS_2 films modified by temporally shaped femtosecond pulses. (g) Typical SEM image of gold NPs on MoS_2 films modified by conventional femtosecond pulses. All scale bars are 500 nm. (h) EDX spectrum, (i) HRTEM image, (j) SAED image, and (k) XRD pattern (d is lattice spacing and D is grain size) of gold NPs decorated on MoS_2 films. Other XRD peaks are indexed to MoS_2 (Figure S6) and do not offer a concrete analysis.

bonds of S atom were broken by femtosecond laser, the S atoms were at an unsaturated or extremely unsaturated state, forming unbound sulfur with dangling bonds; then the valence state of stimulated S atoms was further higher, and the corresponding binding energy further increased to 164.96 eV. Additionally, when abundant S atoms were at unsaturated or extremely unsaturated state (highly excited by laser), the unbound sulfur peak (binding energy at 164.96 eV)[42] would be large, which corresponded to the high chemical activity of femtosecond laser-treated MoS_2. Another indirect evidence to prove the existing of S atoms not forming perfect MoS_2 was atomic concentration ratio of S atoms compared with Mo atoms, and this ratio of MoS_2 surface treated by temporally shaped femtosecond pulses was larger than 2:1 even reaching up to 4.28:1, which indicated the selective removal of abundant Mo atoms by a femtosecond laser. Thus, the area of laser-treated MoS_2 was no longer pure MoS_2, and abundant S atoms were not fully bonded.

Shape-Controllable Gold NPs–MoS_2 Hybrids Prepared by Utilizing Laser-Treated MoS_2. By adjusting the femtosecond pulses parameters (pulse energy, scan speed, and pulse delay), surface chemical activity and surface periodic structures of MoS_2 films were effectively controlled. Gold NPs with three categories of micro/nano structures (which have six kinds of typical shapes) were in situ and self-assembly decorated on MoS_2 films by the reduction reaction of $AuCl_3$ solution within laser-treated MoS_2 regions. The three categories of gold micro/nano structures are as follows: (1) gold sphere including all quasi-spherical NPs (Figure 4a); (2) gold debris including petal-shaped and rice-shaped NPs (Figure 4b,c) and NPs whose shape between the two; (3) gold cluster with hierarchical morphology, such as popcorn-shaped, ricepaper pith-shaped, and flower-shaped NPs (Figure 4d–f). Here, the diversified shapes of gold NPs decorated on MoS_2 surfaces were effectively controlled by modifying MoS_2 surfaces via temporally shaped femtosecond pulses with different parameters (Figure S10). It was found that sphere-shaped gold NPs were mainly generated at low scan speeds (such as 100 μm/s) and short pulse delays (such as 0.1 ps). High scan speeds (such as 2000 μm/s) and long pulse delays (such as 10 ps) generated debris-shaped gold NPs, while cluster-shaped gold NPs were mainly produced at large pulse energies (such as 0.6 μJ). The morphology and size of the six kind typical gold shapes are as follows (laser processing parameters are shown in Table S1): (1) quasi-spherical with diameter of approximately 230 nm (Figure 4a); (2) petal-shaped with length, width, and thickness of approximately 200, 100, and 50 nm, respectively (Figure 4b); (3) rice-shaped with length, width, and thickness of approximately 300, 80, and 50 nm, respectively (Figure 4c); (4) popcorn-shaped with overall dimensions of approximately 550 nm covered with 50–100 nm protrusions (Figure 4d); (5) ricepaper pith-shaped with overall dimensions of approximately 500 nm covered with 50–100 nm protrusions (Figure 4e); (6) flower-shaped with overall dimensions of approximately 800 nm covered with 50–100 nm protrusions (Figure 4f). However, the shapes of gold NPs decorated on MoS_2 films by conventional femtosecond pulses were relatively sole, and only torispherical or irregular spherical particles with wide size distribution ranging from 250 to 750 nm were observed (Figure

DOI: 10.1021/acsami.6b14805
ACS Appl. Mater. Interfaces 2017, 9, 7447–7455

4g). The categories, classification basis, typical morphologies, and size of the gold NPs are summarized in Table S2.

The chemical composition and crystalline nature of the gold NPs decorated on premodified MoS_2 films were investigated using energy dispersive X-ray spectroscopy (EDX), transmission electron microscopy (TEM), and X-ray diffractometer (XRD). Figure 4h shows the EDX spectrum of Au-MoS_2 hybrid films, which qualitatively confirmed the chemical composition of gold. Meanwhile, Figures 4i and 4j show the high-resolution TEM (HRTEM) images and corresponding selected area electron diffraction (SAED) pattern of the gold NPs, respectively (the low-resolution TEM images for the three categories of gold NPs−MoS_2 hybrids are presented in Figures S11−S13), both which demonstrated the high crystallization of gold NPs decorated on MoS_2 film. The SAED pattern identified three diffraction rings assigned to the {111}, {220}, and {311} planes of the face-centered cubic (fcc) lattice of gold. The strongest diffraction ring, the{111} plane with lattice spacing of 0.235 nm, indicated the predominant crystal orientation of gold NPs decorated on laser-treated MoS_2 films, consistent with HRTEM observation of lattice fringe spacing of 0.235 nm. The XRD characterization of Au−MoS_2 hybrid films (Figure 4k) further demonstrated the crystalline nature of gold NPs. Similar to the SAED characterization, three peaks indexed to {111}, {220}, and {311} planes for fcc lattice gold was observed, and the strongest peak indexed to {111} plane indicated the predominant crystal orientation, corresponding lattice spacing of 0.235 nm (calculated by Bragg equation) and grain size of 26.2 nm (calculated by the Scherrer formula). The TEM and XRD results indicated that femtosecond pulse-treated MoS_2 film is conducive to gold NPs growing along its {111} plane.

The polymorphous gold NPs decorated on laser-treated MoS_2 were primarily attributed to two property changes of the laser-treated MoS_2 film, namely the surface reducibility and the surface periodic structures. Surface reducibility of laser-treated MoS_2 was derived from the MoS_2 micro/nano debris which definitely terminated with S atoms (unbound sulfurs), and the unbound sulfurs had unpaired electrons, forming unsaturated bonds which have strong chemical reducibility (Figure 3). When gold cations with oxidizability met unbound sulfurs with strong reducibility, the gold cations were reduced to gold atoms (Figure 5a). However, no gold was reduced from $AuCl_3$ solution on pristine MoS_2 films (Figure S14), indicating that no chemical reduction activity existed on pristine MoS_2 surface. This phenomenon verified that only MoS_2 surface modified by femtosecond pulses can drive the chemical reduction of gold. Furthermore, the high density of gold NPs indicated high chemical activity of laser-treated MoS_2. After gold cations were reduced to gold atoms, which aggregated together to form gold seeding NPs, namely nucleation, the gold seeding NPs continued to grow up with the reduction of more gold atoms, and the surface structures of laser-treated MoS_2 assisted oriented or free growth of gold seeding NPs, leading to larger gold nanostructures with various shapes (Figure 5b,c) via Au^0 crystal incorporation.[47] The detailed growth processes of nonspherical gold NPs, including gold debris and gold cluster, were explored through the investigation of time-dependent morphological changes (Figures S15 and S16). Additionally, the growth process of gold NPs on modified MoS_2 surface by conventional femtosecond pulses were also studied (Figure S17), which indicated that the growth rate of gold NPs on MoS_2 modified by conventional femtosecond pulses was slower than that by temporally shaped femtosecond pulses; this

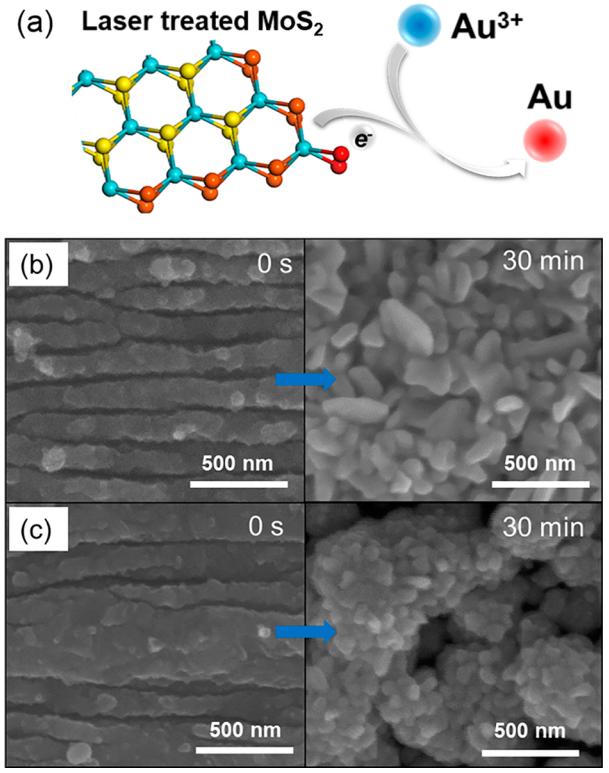

Figure 5. Reduction of gold NPs and the effects of surface structures of MoS_2 on gold morphology. (a) Gold cations were reduced to be gold atoms by laser treated MoS_2. (b) Short-periodic structures and (c) long-periodic structures led to different nonspherical gold NPs ("0 s" and "30 min" represent the reaction time of laser-treated MoS_2 and $AuCl_3$ solution).

difference was attributed to the weaker chemical reduction activity of the modified MoS_2 by conventional femtosecond pulses, eventually leading to only torispherical or irregular spherical gold NPs decorated on MoS_2.

Highly Sensitive and Tunable SERS Application of Obtained Au−MoS_2 Hybrids. Surface-enhanced Raman scattering (SERS) is a powerful microanalytical tool for organic and biological molecules detection due to its unique vibrational fingerprints of the analysts.[24,48−50] SERS has been intensively studied, and the high enhancement factors (EF) of noble metals as dominant SERS substrate material is due to the enhancement of the local electromagnetic fields around metallic structures, called the electromagnetic mechanism (EM) effect.[48] However, recent research suggests that most two-dimensional (2D) materials (such as graphene, h-BN, MoS_2, g-C_3N_4, etc.) provide a good choice as an ideal flat substrate for SERS, the SERS of which is dominated by the chemical mechanism (such as charge transfer effect between organic molecules and material) rather than the electromagnetic mechanism, and they are easy to combine with traditional metallic substrates, which allows us to take advantage of both metal substrates and 2D material substrates.[48,51,52] Therefore, the SERS research of noble metal−MoS_2 hybrids is on the upgrade in recent years,[24,25,27] showing great potential as an excellent SERS substrate, although their Raman enhancement factor is lower than the published highest EF of traditional metallic substrates.

Here, the obtained Au−MoS_2 hybrids with shape-controlled gold NPs were applied as SERS substrates to explore their SERS activity, using R6G as probe molecules. The Au−MoS_2

DOI: 10.1021/acsami.6b14805
ACS Appl. Mater. Interfaces 2017, 9, 7447−7455

hybrid films were dropped with R6G aqueous solution with concentration of 1×10^{-6} M/L for Raman signal detection. For comparison, the smooth bare MoS_2 film were dropped with R6G aqueous solution with concentration of 1×10^{-2} M/L for Raman signal detection. The R6G molecules can be adsorbed onto hybrid films, which might be due to the S−π coordination interaction between R6G and MoS_2 (a more detailed analysis is provided in the Supporting Information and Figures S18−S21). Raman spectra of R6G on Au−MoS_2 hybrids with three categories of gold shapes (debris shape, cluster shape, and sphere shape) and bare MoS_2 film are shown in Figures 6a, 6b, 6c, and 6e, respectively. To quantitatively analyzing the enhancement effect, the EF was calculated by selecting the Raman peak located at 1363 cm^{-1} (the assignments of the main bands of R6G are shown in Table S3). The calculation formula is referred to the previous report,[24,25] as shown in eq 1

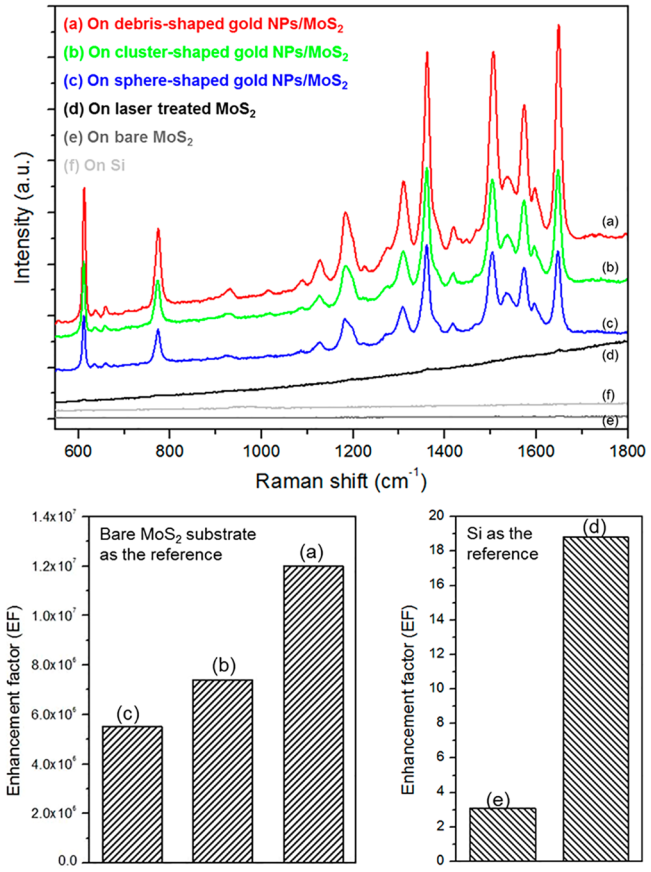

Figure 6. Raman spectra of R6G (top) and EF (bottom) calculated on three categories of Au−MoS_2 hybrids, laser-treated MoS_2 film, MoS_2 film, and Si: (a) on debris-shaped Au−MoS_2 hybrids (red line), (b) on cluster-shaped Au−MoS_2 hybrids (green line), (c) on sphere-shaped Au−MoS_2 hybrids (blue line), (d) on laser-treated MoS_2 film (black line), (e) on bare MoS_2 film (gray line), and (f) on Si surface (light gray line).

$$EF = \frac{I_{SERS}}{I_{ref}} \frac{N_{ref}}{N_{SERS}} \quad (1)$$

where the Raman spectra of R6G molecules on bare MoS_2 substrate is as the reference. The calculated EFs of the sphere-shaped, cluster-shaped, and debris-shaped Au−MoS_2 hybrids were respectively 5.5×10^6, 7.4×10^6, and 1.2×10^7, to our best acquaintance, which is the highest EF of Au−MoS_2 hybrids as Raman-active surfaces, showing the highly sensitive and tunable SERS activity.

In addition, we compared the Raman signal of R6G on Si (as comparison) with the SERS spectrum of R6G on pristine and laser-treated MoS_2 to understand the chemical enhancement of laser-treated MoS_2. To calculate the Raman EF, we selected the intensity of the Raman signals at 1363 cm^{-1} and Raman signal of R6G on Si as reference. It turned out that the EF for R6G on MoS_2 was approximately 3.1, and that for R6G on laser-treated MoS_2 was approximately 18.8. This demonstrates that there was a Raman enhancement effect on the surface of MoS_2 and a higher Raman enhancement effect on the surface of laser-treated MoS_2. Because of the S−π coordination interaction between MoS_2 and R6G, charge transfer can easily occur between MoS_2 and the adsorbed molecules, which would induce chemical enhancement. Meanwhile, MoS_2 is semiconducting with the sulfur atoms on its surface and has a polar covalent bond (Mo−S) with the polarity in the vertical direction to the surface; hence, both charge transfer and dipole−dipole coupling may occur.[48] This interface dipole−dipole interaction could also induce a significant Raman enhancement. Furthermore, the surface modification of laser-treated MoS_2 changed its local surface properties: introducing defects (forming unbound sulfur that can easily combine with R6G through S−π coordination interaction) which can result in enhanced charge transfer effect; creating local dipoles which can improve the interface dipole−dipole coupling.

According to the analysis, the high EF for Au−MoS_2 hybrids in this work was attributed to three aspects. (1) Morphology of gold NPs decorated on MoS_2: local electromagnetic fields were enhanced around gold structures, generally called "hot spots", and nonspherical gold nanostructures had higher local electromagnetic field enhancement, where nonspherical tips formed sharp peaks and nonuniform configuration increased the surface-to-volume ratio, leading to an enhanced Raman scattering[49] (detailed analysis about the effect of different gold shape on EM enhancement is provided in the Supporting Information). (2) Femtosecond laser modification of the MoS_2 surface: surface modification of MoS_2 by femtosecond laser changed its local surface properties, such as introducing defects and creating local dipoles, which resulted in enhanced charge transfer effect and interface dipole−dipole coupling between R6G molecules and MoS_2. (3) Surface periodic structures of the MoS_2 substrates: the induced surface periodic structures increased the surface roughness of MoS_2 films, which facilitated the generation of "hot spots".[53] In addition, we did experiments to test the reproducibility, stability, uniformity, and adaptability of our Au−MoS_2 hybrids as SERS substrates (more details are provided in the Supporting Information and Figures S22−S25).

CONCLUSIONS

A novel method was proposed to nonthermally induce edge-active sites (unbound sulfur) and surface periodic micro/nano structures on MoS_2 films via temporally shaped femtosecond pulses. High-crystalline and shape-controlled gold NPs were in situ and self-assembly grown on modified MoS_2 films in $AuCl_3$ solution without any reduction agents. Raman, XPS, and AFM characterization indicated that the chemical reduction ability of modified MoS_2 resulted from the nonthermally tuned MoS_2 edge-active sites with sulfur terminal induced by femtosecond pulse. The combined roles of tunable active sites and periodic micro/nano structures on laser-treated MoS_2 surface determined the shapes of the gold nanostructures. In addition,

DOI: 10.1021/acsami.6b14805
ACS Appl. Mater. Interfaces 2017, 9, 7447−7455

compared with conventional femtosecond pulses, temporally shaped femtosecond pulse modified MoS_2 presented higher ratios of unbound sulfur, higher chemical reducibility, and faster reaction rates, resulting in diversified shapes of gold NPs. Furthermore, the Au−MoS_2 hybrids exhibited highly sensitive and tunable SERS activity with an enhancement factor reaching up to 1.2×10^7, demonstrating a great potential for future chemical and biological sensing applications.

METHODS

Temporally Shaped Femtosecond Pulse Modification. The temporally shaped femtosecond pulse processing system was based on Michelson interferometer. The femtosecond laser pulse was emitted from a 35 fs Ti:sapphire laser system operating at wavelength and repetition rate of 800 nm and 1 kHz, respectively. The delay time between double subpulses could be tuned ranging from femtoseconds to tens of picoseconds by the position of mobile mirror driven by a linear translation stage. The laser beam was focused with a 5× Olympus microscope objective (NA = 0.15) and incident normal to the surface of samples placed on a six-axis translation stage (M-840.5DG, PI, Inc.).

Preparation of Au−MoS_2 Hybrids. $AuCl_3$ solution with concentration of 2.1 mM/L provided the raw material for self-assembly of gold nanostructures. The premodified MoS_2 films were directly immersed in the $AuCl_3$ solution for 30 min. Subsequently, the MoS_2 films decorated with gold NPs were taken out for natural air drying.

Characterization of MoS_2 and Decorated Gold NPs. The surface morphology and energy dispersive X-ray spectroscopy (EDX) were investigated using a scanning electron microscope (SEM, FEI Quanta 200 FEG). The transmission electron microscopy (TEM) was performed using a JEM-2100 TEM. The X-ray diffraction analysis was performed using a parallel beam Bruker D8 Advance X-ray diffractometer (XRD). Raman and photoluminescence (PL) spectra were obtained using a Renishaw InVia Reflex spectrometer with a 532 nm light source. X-ray photoelectron spectroscopy (XPS) was carried out using a PHI Quantera X-ray photoelectron spectrometer. The atomic force microscope (AFM) characterization was performed using a SPM-960 AFM.

SERS Activity of the Au−MoS_2 Hybrids. SERS was performed by detecting R6G molecules via a Renishaw InVia Reflex spectrometer with 532 and 633 nm light source.

ASSOCIATED CONTENT

Supporting Information

The Supporting Information is available free of charge on the ACS Publications website at DOI: 10.1021/acsami.6b14805.

> Characterizations of pristine MoS_2 films; extended Raman and XPS spectrums; morphology distribution of gold NPs; processing parameters of laser; table about the categories, classification basis, typical morphologies, and size of gold NPs; extended TEM figures; extended SEM analysis; analysis about interaction between R6G and laser-treated MoS_2; Raman frequencies (cm^{-1}) and assignments of the main bands of R6G; analysis about the effect of different gold shape on EM enhancement; reproducibility, stability, uniformity, and adaptability tests of Au−MoS_2 hybrids as a SERS substrate (PDF)

AUTHOR INFORMATION

Corresponding Author

*(L.J.) E-mail: jianglan@bit.edu.cn.

ORCID

Lan Jiang: 0000-0003-0488-1987

Notes

The authors declare no competing financial interest.

ACKNOWLEDGMENTS

The research was supported by the National Natural Science Foundation of China (NSFC) (Grant 91323301) and the National Basic Research Program of China (973 Program) (Grant 2011CB013000).

REFERENCES

(1) Bonaccorso, F.; Colombo, L.; Yu, G.; Stoller, M.; Tozzini, V.; Ferrari, A. C.; Ruoff, R. S.; Pellegrini, V. Graphene, Related Two-Dimensional Crystals, and Hybrid Systems for Energy Conversion and Storage. *Science* **2015**, *347*, 1246501.

(2) Xu, M.; Liang, T.; Shi, M.; Chen, H. Graphene-like Two-Dimensional Materials. *Chem. Rev.* **2013**, *113*, 3766−3798.

(3) Butler, S. Z.; Hollen, S. M.; Cao, L.; Cui, Y.; Gupta, J. A.; Gutiérrez, H. R.; Heinz, T. F.; Hong, S. S.; Huang, J.; Ismach, A. F.; et al. Progress, Challenges, and Opportunities in Two-Dimensional Materials Beyond Graphene. *ACS Nano* **2013**, *7*, 2898−2926.

(4) Suzuki, R.; Sakano, M.; Zhang, Y.; Akashi, R.; Morikawa, D.; Harasawa, A.; Yaji, K.; Kuroda, K.; Miyamoto, K.; Okuda, T.; et al. Valley-Dependent Spin Polarization in Bulk MoS_2 with Broken Inversion Symmetry. *Nat. Nanotechnol.* **2014**, *9*, 611−617.

(5) Radisavljevic, B.; Radenovic, A.; Brivio, J.; Giacometti, V.; Kis, A. Single-Layer MoS_2 Transistors. *Nat. Nanotechnol.* **2011**, *6*, 147−150.

(6) Wu, H.; Yang, R.; Song, B.; Han, Q.; Li, J.; Zhang, Y.; Fang, Y.; Tenne, R.; Wang, C. Biocompatible Inorganic Fullerene-like Molybdenum Disulfide Nanoparticles Produced by Pulsed Laser Ablation in Water. *ACS Nano* **2011**, *5*, 1276−1281.

(7) Kiriya, D.; Lobaccaro, P.; Nyein, H. Y. Y.; Taheri, P.; Hettick, M.; Shiraki, H.; Sutter-Fella, C. M.; Zhao, P.; Gao, W.; Maboudian, R. General Thermal Texturization Process of MoS_2 for Efficient Electrocatalytic Hydrogen Evolution Reaction. *Nano Lett.* **2016**, *16*, 4047−4053.

(8) Karunadasa, H. I.; Montalvo, E.; Sun, Y.; Majda, M.; Long, J. R.; Chang, C. J. A Molecular MoS_2 Edge Site Mimic for Catalytic Hydrogen Generation. *Science* **2012**, *335*, 698−702.

(9) Jaramillo, T. F.; Jørgensen, K. P.; Bonde, J.; Nielsen, J. H.; Horch, S.; Chorkendorff, I. Identification of Active Edge Sites for Electrochemical H_2 Evolution from MoS_2 Nanocatalysts. *Science* **2007**, *317*, 100−102.

(10) Voiry, D.; Salehi, M.; Silva, R.; Fujita, T.; Chen, M.; Asefa, T.; Shenoy, V. B.; Eda, G.; Chhowalla, M. Conducting MoS_2 Nanosheets as Catalysts for Hydrogen Evolution Reaction. *Nano Lett.* **2013**, *13*, 6222−6227.

(11) Cui, S.; Wen, Z.; Huang, X.; Chang, J.; Chen, J. Stabilizing MoS_2 Nanosheets through SnO_2 Nanocrystal Decoration for High-Performance Gas Sensing in Air. *Small* **2015**, *11*, 2305−2313.

(12) Yu, X.; Shiraki, T.; Yang, S.; Ding, B.; Nakashima, N. Synthesis of Porous Gold Nanoparticle/MoS_2 Nanocomposites Based on Redox Reactions. *RSC Adv.* **2015**, *5*, 86558−86563.

(13) Lee, J.; Dak, P.; Lee, Y.; Park, H.; Choi, W.; Alam, M. A.; Kim, S. Two-Dimensional Layered MoS_2 Biosensors Enable Highly Sensitive Detection of Biomolecules. *Sci. Rep.* **2014**, *4*, 7352.

(14) Dai, W.; Dong, H.; Fugetsu, B.; Cao, Y.; Lu, H.; Ma, X.; Zhang, X. Tunable Fabrication of Molybdenum Disulfide Quantum Dots for Intracellular Micro RNA Detection and Multiphoton Bioimaging. *Small* **2015**, *11*, 4158−4164.

(15) Wu, W.; Wang, L.; Li, Y.; Zhang, F.; Lin, L.; Niu, S.; Chenet, D.; Zhang, X.; Hao, Y.; Heinz, T. F. Piezoelectricity of Single-Atomic-Layer MoS_2 for Energy Conversion and Piezotronics. *Nature* **2014**, *514*, 470−474.

(16) Li, H.; Tsai, C.; Koh, A. L.; Cai, L.; Contryman, A. W.; Fragapane, A. H.; Zhao, J.; Han, H. S.; Manoharan, H. C.; Abild-Pedersen, F. Activating and Optimizing MoS_2 Basal Planes for Hydrogen Evolution through the Formation of Strained Sulphur Vacancies. *Nat. Mater.* **2015**, *15*, 48−53.

DOI: 10.1021/acsami.6b14805
ACS Appl. Mater. Interfaces 2017, 9, 7447−7455

(17) Hansen, L. P.; Ramasse, Q. M.; Kisielowski, C.; Brorson, M.; Johnson, E.; Topsøe, H.; Helveg, S. Atomic-Scale Edge Structures on Industrial-Style MoS_2 Nanocatalysts. *Angew. Chem., Int. Ed.* **2011**, *50*, 10153−10156.
(18) Yu, Y.; Huang, S.-Y.; Li, Y.; Steinmann, S. N.; Yang, W.; Cao, L. Layer-Dependent Electrocatalysis of MoS_2 for Hydrogen Evolution. *Nano Lett.* **2014**, *14*, 553−558.
(19) Xie, J.; Zhang, H.; Li, S.; Wang, R.; Sun, X.; Zhou, M.; Zhou, J.; Lou, X. W. D.; Xie, Y. Defect-Rich MoS_2 Ultrathin Nanosheets with Additional Active Edge Sites for Enhanced Electrocatalytic Hydrogen Evolution. *Adv. Mater.* **2013**, *25*, 5807−5813.
(20) Lukowski, M. A.; Daniel, A. S.; Meng, F.; Forticaux, A.; Li, L.; Jin, S. Enhanced Hydrogen Evolution Catalysis from Chemically Exfoliated Metallic MoS_2 Nanosheets. *J. Am. Chem. Soc.* **2013**, *135*, 10274−10277.
(21) Shi, Y.; Wang, J.; Wang, C.; Zhai, T.-T.; Bao, W.-J.; Xu, J.-J.; Xia, X.-H.; Chen, H.-Y. Hot Electron of Au Nanorods Activates the Electrocatalysis of Hydrogen Evolution on MoS_2 Nanosheets. *J. Am. Chem. Soc.* **2015**, *137*, 7365−7370.
(22) Butun, S.; Tongay, S.; Aydin, K. Enhanced Light Emission from Large-Area Monolayer MoS_2 Using Plasmonic Nanodisc Arrays. *Nano Lett.* **2015**, *15*, 2700−2704.
(23) Yin, Z.; Chen, B.; Bosman, M.; Cao, X.; Chen, J.; Zheng, B.; Zhang, H. Au Nanoparticle-Modified MoS_2 Nanosheet-Based Photoelectrochemical Cells for Water Splitting. *Small* **2014**, *10*, 3537−3543.
(24) Su, S.; Zhang, C.; Yuwen, L.; Chao, J.; Zuo, X.; Liu, X.; Song, C.; Fan, C.; Wang, L. Creating SERS Hot Spots on MoS_2 Nanosheets with In Situ Grown Gold Nanoparticles. *ACS Appl. Mater. Interfaces* **2014**, *6*, 18735−18741.
(25) Lu, J.; Lu, J. H.; Liu, H.; Liu, B.; Gong, L.; Tok, E. S.; Loh, K. P.; Sow, C. H. Microlandscaping of Au Nanoparticles on Few-Layer MoS_2 Films for Chemical Sensing. *Small* **2015**, *11*, 1792−1800.
(26) Kang, Y.; Najmaei, S.; Liu, Z.; Bao, Y.; Wang, Y.; Zhu, X.; Halas, N. J.; Nordlander, P.; Ajayan, P. M.; Lou, J.; Fang, Z. Plasmonic Hot Electron Induced Structural Phase Transition in a MoS_2 Monolayer. *Adv. Mater.* **2014**, *26*, 6467−6471.
(27) Daeneke, T.; Carey, B.; Chrimes, A.; Ou, J. Z.; Lau, D.; Gibson, B.; Bhaskaran, M.; Kalantar-Zadeh, K. Light Driven Growth of Silver Nanoplatelets on 2D MoS_2 Nnanosheet Templates. *J. Mater. Chem. C* **2015**, *3*, 4771−4778.
(28) Mukherjee, B.; Simsek, E. Plasmonics Enhanced Average Broadband Absorption of Monolayer MoS_2. *Plasmonics* **2016**, *11*, 285−289.
(29) Yu, Y.; Ji, Z.; Zu, S.; Du, B.; Kang, Y.; Li, Z.; Zhou, Z.; Shi, K.; Fang, Z. Ultrafast Plasmonic Hot Electron Transfer in Au Nanoantenna/MoS_2 Heterostructures. *Adv. Funct. Mater.* **2016**, *26*, 6394−6401.
(30) Zhao, J.; Zhang, Z.; Yang, S.; Zheng, H.; Li, Y. Facile Synthesis of MoS_2 Nanosheet-Silver Nanoparticles Composite for Surface Enhanced Raman Scattering and Electrochemical Activity. *J. Alloys Compd.* **2013**, *559*, 87−91.
(31) Li, X.; Zhu, J.; Wei, B. Hybrid Nanostructures of Metal/Two-Dimensional Nanomaterials for Plasmon-Enhanced Applications. *Chem. Soc. Rev.* **2016**, *45* (11), 3145−3187.
(32) Yuwen, L.; Xu, F.; Xue, B.; Luo, Z.; Zhang, Q.; Bao, B.; Su, S.; Weng, L.; Huang, W.; Wang, L. General Synthesis of Noble Metal (Au, Ag, Pd, Pt) Nanocrystal Modified MoS_2 Nanosheets and the Enhanced Catalytic Activity of Pd-MoS_2 for Methanol Oxidation. *Nanoscale* **2014**, *6*, 5762−5769.
(33) Huang, X.; Zeng, Z.; Bao, S.; Wang, M.; Qi, X.; Fan, Z.; Zhang, H. Solution-Phase Epitaxial Growth of Noble Metal Nanostructures on Dispersible Single-Layer Molybdenum Disulfide Nanosheets. *Nat. Commun.* **2013**, *4*, 1444.
(34) Connelly, N. G.; Geiger, W. E. Chemical Redox Agents for Organometallic Chemistry. *Chem. Rev.* **1996**, *96* (2), 877−910.
(35) Kennedy, L. C.; Bickford, L. R.; Lewinski, N. A.; Coughlin, A. J.; Hu, Y.; Day, E. S.; West, J. L.; Drezek, R. A. A New Era for Cancer Treatment: Gold-Nanoparticle-Mediated Thermal Therapies. *Small* **2011**, *7* (2), 169−183.
(36) Ha, H. D.; Han, D. J.; Choi, J. S.; Park, M.; Seo, T. S. Dual Role of Blue Luminescent MoS_2 Quantum Dots in Fluorescence Resonance Energy Transfer Phenomenon. *Small* **2014**, *10* (19), 3858−3862.
(37) Yu, S. H.; Lee, Y.; Jang, S. K.; Kang, J.; Jeon, J.; Lee, C.; Lee, J. Y.; Kim, H.; Hwang, E.; Lee, S.; Cho, J. H. Dye-Sensitized MoS_2 Photodetector with Enhanced Spectral Photoresponse. *ACS Nano* **2014**, *8* (8), 8285−8291.
(38) Ganatra, R.; Zhang, Q. Few-Layer MoS_2: a Promising Layered Semiconductor. *ACS Nano* **2014**, *8*, 4074−4099.
(39) Paradisanos, I.; Kymakis, E.; Fotakis, C.; Kioseoglou, G.; Stratakis, E. Intense Femtosecond Photoexcitation of Bulk and Monolayer MoS_2. *Appl. Phys. Lett.* **2014**, *105*, 041108.
(40) Shi, X.; Li, X.; Jiang, L.; Qu, L.; Zhao, Y.; Ran, P.; Wang, Q.; Cao, Q.; Ma, T.; Lu, Y. Femtosecond Laser Rapid Fabrication of Large-Area Rose-like Micropatterns on Freestanding Flexible Graphene Films. *Sci. Rep.* **2015**, *5*, 17557.
(41) Bonse, J.; Baudach, S.; Krüger, J.; Kautek, W.; Lenzner, M. Femtosecond Laser Ablation of Silicon-Modification Thresholds and Morphology. *Appl. Phys. A: Mater. Sci. Process.* **2002**, *74* (1), 19−25.
(42) Si, P.; Chi, Q.; Li, Z.; Ulstrup, J.; Møller, P. J.; Mortensen, J. Functional Polythiophene Nanoparticles: Size-Controlled Electropolymerization and Ion Selective Response. *J. Am. Chem. Soc.* **2007**, *129*, 3888−3896.
(43) Yokoyama, T.; Imanishi, A.; Terada, S.; Namba, H.; Kitajima, Y.; Ohta, T. Electronic Properties of SO_2 Adsorbed on Ni (100) Studied by UPS and O K-Edge NEXAFS. *Surf. Sci.* **1995**, *334*, 88−94.
(44) Chang, K.; Mei, Z.; Wang, T.; Kang, Q.; Ouyang, S.; Ye, J. MoS_2/Graphene Cocatalyst for Efficient Photocatalytic H_2 Evolution under Visible Light Irradiation. *ACS Nano* **2014**, *8*, 7078−7087.
(45) Assion, A.; Baumert, T.; Bergt, M.; Brixner, T.; Kiefer, B.; Seyfried, V.; Strehle, M.; Gerber, G. Control of Chemical Reactions by Feedback-Optimized Phase-Shaped Femtosecond Laser Pulses. *Science* **1998**, *282*, 919−922.
(46) Levis, R. J.; Menkir, G. M.; Rabitz, H. Selective Bond Dissociation and Rearrangement with Optimally Tailored, Strong-Field Laser Pulses. *Science* **2001**, *292*, 709−713.
(47) Sreeprasad, T.; Nguyen, P.; Kim, N.; Berry, V. Controlled, Defect-Guided, Metal-Nanoparticle Incorporation onto MoS_2 via Chemical and Microwave Routes: Electrical, Thermal, and Structural Properties. *Nano Lett.* **2013**, *13* (9), 4434−4441.
(48) Ling, X.; Fang, W.; Lee, Y.-H.; Araujo, P. T.; Zhang, X.; Rodriguez-Nieva, J. F.; Lin, Y.; Zhang, J.; Kong, J.; Dresselhaus, M. S. Raman Enhancement Effect on Two-Dimensional Layered Materials: Graphene, h-BN and MoS_2. *Nano Lett.* **2014**, *14*, 3033−3040.
(49) Zhang, Y.; Wang, B.; Yang, S.; Li, L.; Guo, L. Facile Synthesis of Spinous-like Au Nanostructures for Unique Localized Surface Plasmon Resonance and Surface-Enhanced Raman Scattering. *New J. Chem.* **2015**, *39*, 2551−2556.
(50) Jiang, J.; Ou-Yang, L.; Zhu, L.; Zou, J.; Tang, H. Novel One-Pot Fabrication of Lab-on-a-Bubble@Ag Substrate without Coupling-Agent for Surface Enhanced Raman Scattering. *Sci. Rep.* **2014**, *4*, 3942.
(51) Sun, L.; Hu, H.; Zhan, D.; Yan, J.; Liu, L.; Teguh, J. S.; Yeow, E. K.; Lee, P. S.; Shen, Z. Plasma Modified MoS_2 Nanoflakes for Surface Enhanced Raman Scattering. *Small* **2014**, *10*, 1090−1095.
(52) Jiang, J.; Zhu, L.; Zou, J.; Ou-yang, L.; Zheng, A.; Tang, H. Micro/Nano-Structured Graphitic Carbon Nitride-Ag Nanoparticle Hybrids as Surface-Enhanced Raman Scattering Substrates with Much Improved Long-Term Stability. *Carbon* **2015**, *87*, 193−205.
(53) Yang, Q.; Li, X.; Jiang, L.; Zhang, N.; Zhang, G.; Shi, X.; Zhang, K.; Hu, J.; Lu, Y. Nanopillar Arrays with Nanoparticles Fabricated by a Femtosecond Laser Pulse Train for Highly Sensitive SERRS. *Opt. Lett.* **2015**, *40*, 2045−2048.

DOI: 10.1021/acsami.6b14805
ACS Appl. Mater. Interfaces 2017, 9, 7447−7455